Mon. Not. R. Astron. Soc. **339,** 515–523 (2003)

Uniformly rotating axisymmetric fluid configurations bifurcating from highly flattened Maclaurin spheroids

Marcus Ansorg,★ Andreas Kleinwächter and Reinhard Meinel
Theoretisch-Physikalisches Institut, University of Jena, Max-Wien-Platz 1, 07743 Jena, Germany

Accepted 2002 October 18. Received 2002 October 10; in original form 2002 August 14

ABSTRACT

We present a thorough investigation of sequences of uniformly rotating, homogeneous axisymmetric Newtonian equilibrium configurations that bifurcate from highly flattened Maclaurin spheroids. Each one of these sequences possesses a mass-shedding limit. Starting at this point, the sequences proceed towards the Maclaurin sequence and beyond. The first sequence leads to the well-known Dyson rings, whereas the end-points of the higher sequences are characterized by the formation of a two-body system, either a core–ring system (for the second, the fourth, etc., sequence) or a two-ring system (for the third, the fifth, etc., sequence). Although the general qualitative picture drawn by Eriguchi and Hachisu in the 1980s has been confirmed, slight differences arise in the interpretation of the origin of the first two-ring sequence and in the general appearance of fluid bodies belonging to higher sequences.

Key words: gravitation – hydrodynamics – methods: numerical – stars: rotation.

1 INTRODUCTION AND OVERVIEW

If one moves along the Maclaurin sequence of uniformly rotating, axisymmetric, homogeneous fluid ellipsoids with fixed mass and fixed density, starting at the non-rotating configuration and proceeding towards increasing angular momentum, one first encounters the Jacobi branch point where the Maclaurin spheroids become secularly unstable with regard to the first non-axisymmetric perturbation (see e.g. Chandrasekhar 1969). The corresponding Jacobi sequence branching off at this point leads to further bifurcations, in particular to Poincaré's 'pear-shaped' sequence (see Eriguchi & Hachisu 1982b). Farther along the Maclaurin path, one next comes to the bifurcation points of the non-axisymmetric 'triangle', 'square' and 'ammonite' sequences (Chandrasekhar 1969; Eriguchi & Hachisu 1982a), before one arrives at the first axisymmetric sequence bifurcating at an eccentricity $\varepsilon_1 = 0.985\,23$ (Chandrasekhar 1967; Bardeen 1971). As conjectured by Bardeen (1971) and confirmed by Eriguchi & Sugimoto (1981), the bodies of this sequence pinch together gradually at the centre and eventually form the anchor–ring configurations studied by Dyson (1892, 1893) and Wong (1974); see also Poincaré (1885a,b,c), Kowalewsky (1895), Lichtenstein (1933) and a somewhat related paper by Kley (1996).

Another not yet confirmed conjecture by Bardeen (1971) concerns a sequence of axisymmetric 'central-bulge' configurations likewise bifurcating at ε_1. In this paper we indeed found this sequence, which might be considered to be a continuation of the Dyson ring sequence beyond the Maclaurin spheroids and ends in a mass-shedding limit. However, the surface shapes of the corresponding fluid bodies do not generate a 'central-bulge' region; their appearance is more 'lens-shaped'.

★E-mail: ansorg@tpi.uni-jena.de

Apart from the study of the Dyson ring sequence we shall give a detailed analysis of the next axisymmetric sequences bifurcating from the Maclaurin spheroids. The first core–ring sequence branches off at $\varepsilon_2 = 0.993\,75$. Starting at a mass-shedding limit, this sequence proceeds towards the Maclaurin sequence and beyond, finally leading to the formation of a core–ring system.

In contrast to the results by Eriguchi & Hachisu (1982a), who stated that the first two-ring sequence branches off at ε_2, we found that the bifurcation occurs at $\varepsilon_3 = 0.996\,57$. Again, a mass-shedding limit marks one end-point of this sequence, leading from here towards and beyond the Maclaurin sequence and ending in the formation of a two-ring system.

The same qualitative picture repeats as one moves to the higher axisymmetric bifurcation points at $\varepsilon_4 = 0.997\,84$, $\varepsilon_5 = 0.998\,51$, etc., of which there are infinitely many, accumulating at $\varepsilon = 1$ (Bardeen 1971). Starting at a mass-shedding limit, the sequences proceed towards the Maclaurin sequence and beyond, leading eventually to the formation of a core–ring system for ε_{2l} and a two-ring system for ε_{2l+1} (see Figs 7–11). The body's surface is characterized by a particular number of grooves, notably l, for configurations close to the two-body systems that are the end-stages of the sequences bifurcating at ε_{2l} and ε_{2l+1}. The outermost groove pinches together first and an outer ring without grooves separates. In some continuation process beyond this formation of a two-body system, the other grooves might also pinch off, leading eventually to a multibody system, at most consisting of a core and l rings or $(l + 1)$ rings respectively.[1] However, since a continuation process of this kind is not unique, we

[1] This result is in contrast to the statement by Eriguchi & Hachisu (1982a), who expected the formation of k rings for the ε_k sequence.

consider the sequences in question precisely up to the formation of the two-body system.

These investigations have been carried out up to the ε_{10} sequence. The corresponding final configurations, when the two-body system is formed, can be seen in Figs 7–11 .

Representative plots of physical quantities as well as of meridional cross-sections have been provided up to the ε_5 sequence (see Figs 1–10). Note that the Maclaurin sequence becomes dynamically unstable with respect to axisymmetric perturbations for $\varepsilon > 0.998\,56$ (Bardeen 1971; Eriguchi & Hachisu 1985). Therefore, if we restrict our considerations to axial symmetry, the sequences bifurcating at $\varepsilon_1, \varepsilon_2, \ldots, \varepsilon_5$ are more relevant than those branching off at $\varepsilon_6, \varepsilon_7, \ldots$ ($\varepsilon_k \geqslant \varepsilon_6 = 0.998\,91$ for $k > 5$).

Table 1 lists physical quantities for the Maclaurin spheroids at the bifurcation points ε_k for $k = 1, 2, \ldots, 10$. Tables 2–4 contain numerical data with an accuracy of five digits for configurations of the ε_1, ε_2 and ε_3 sequences. Additionally, Table 5 lists the ratios of the masses of the inner to the outer body at the two-body formation point for the $\varepsilon_2, \ldots, \varepsilon_5$ sequences.

2 BIFURCATION POINTS OF AXISYMMETRIC SEQUENCES

In this section we review the results by Bardeen (1971) who obtained all bifurcation points on the Maclaurin sequence which correspond to axisymmetric perturbations. For our purposes, we will use the Maclaurin spheroids at these points as initial solutions for finding the respective sequence branching off.

The solution Φ of the axisymmetric Poisson equation

$$\Delta\Phi = 4\pi G\mu, \tag{1}$$

where G is Newton's gravitational constant, μ the mass density and Δ the Laplace operator, given in cylindrical coordinates (ρ, ζ) by

$$\Delta = \frac{\partial^2}{\partial\rho^2} + \frac{1}{\rho}\frac{\partial}{\partial\rho} + \frac{\partial^2}{\partial\zeta^2},$$

can be written in the form (Morse & Feshbach 1953)

$$\begin{aligned}\Phi(\xi,\eta) = {} & -2\pi a_0^2 G \sum_{l=0}^{\infty}(2l+1)P_l(\eta) \\ & \times \left[p_l(\xi)\int_{\xi}^{\infty}\int_{-1}^{1}(\xi'^2+\eta'^2)P_l(\eta')q_l(\xi')\mu(\xi',\eta')\,\mathrm{d}\eta'\,\mathrm{d}\xi' \right. \\ & \left. + q_l(\xi)\int_{0}^{\xi}\int_{-1}^{1}(\xi'^2+\eta'^2)P_l(\eta')p_l(\xi')\mu(\xi',\eta')\,\mathrm{d}\eta'\,\mathrm{d}\xi' \right].\end{aligned}$$

Here, the oblate spheroidal coordinates ξ and η are connected with ρ and ζ by

$$\rho = a_0\sqrt{(1+\xi^2)(1-\eta^2)}, \qquad \zeta = a_0\xi\eta.$$

The functions P_l are Legendre polynomials, and the functions p_l and q_l are defined by

$$p_l(\xi) = (-\mathrm{i})^l P_l(\mathrm{i}\xi), \qquad q_l(\xi) = p_l(\xi)\int_{\xi}^{\infty}\frac{\mathrm{d}\xi'}{(1+\xi'^2)[p_l(\xi')]^2}.$$

A fluid body revolving with uniform angular velocity Ω is in hydrostatic equilibrium if the condition

$$\Phi(\xi,\eta) - \tfrac{1}{2}\Omega^2\rho^2 = \Phi_0 = \text{constant} \tag{2}$$

is satisfied at every point of the body's surface.

In order to derive the Maclaurin solutions, one simply starts with an ellipsoidal shape of the surface characterized by $\xi_{\mathrm{S}}(\eta) = \xi_0 =$ constant and moreover takes a_0 to be the corresponding focal length. The density μ vanishes for $\xi > \xi_0$ and is a positive constant if $\xi < \xi_0$, which in the following we simply call μ. Then the resulting surface potential reads as

$$\Phi(\xi_0,\eta) = -\tfrac{4}{3}\pi a_0^2 G\mu\xi_0\left(1+\xi_0^2\right)[q_0(\xi_0) + q_2(\xi_0)P_2(\eta)],$$

and the surface condition (2) indeed is satisfied, provided that Ω and Φ_0 are well-defined functions of a_0, ξ_0 and μ which can be read off from (2).

If we now consider an axisymmetric perturbation of the above Maclaurin shape

$$\xi_{\mathrm{S}}(\eta) = \xi_0 + \kappa\xi_1(\eta) + \mathcal{O}(\kappa^2),$$

insert the corresponding surface potential into the condition (2) and linearize the resulting expression with respect to the small parameter κ, we uniquely find a neighbouring Maclaurin spheroid unless

$$2p_{2k+2}(\xi_0)q_{2k+2}(\xi_0) = \frac{\xi_0}{p_2(\xi_0)}[1 - 2\xi_0 q_2(\xi_0)] \tag{3}$$

is valid for some $k \in \{1, 2, 3, \ldots\}$. The corresponding eccentricity ε_k belonging to the root $\xi_0^{(k)}$ of the above equation is given by

$$\varepsilon_k = \frac{1}{\sqrt{1+\left[\xi_0^{(k)}\right]^2}}, \qquad k = 1, 2, 3, \ldots$$

and marks the bifurcation point on the Maclaurin sequence at which the kth axisymmetric sequence branches off. The numerical values of the first ten ε_k are given in Table 1. As illustrated in Section 4, the bifurcation points appear as cross-over points of the respective sequence with the Maclaurin sequence if one plots the evolution of these sequences in an appropriate parameter diagram (such as angular velocity against the ratio of polar and equatorial radii). Note that the corresponding linear surface displacement $\xi_1^{(k)}$ turns out to be

$$\xi_1^{(k)}(\eta) \propto \frac{P_{2k+2}(\eta)}{\left[\xi_0^{(k)}\right]^2 + \eta^2}. \tag{4}$$

3 NUMERICAL METHODS

The Poisson integral

$$\Phi(\boldsymbol{r}) = -G\mu\int_V \frac{\mathrm{d}^3\boldsymbol{r}'}{|\boldsymbol{r}-\boldsymbol{r}'|}$$

Table 1. Physical quantities for the Maclaurin spheroids at the bifurcation points ε_k. For the definition of ω^2, j^2, T and W, see Section 4.

k	ε_k	Axis ratio	ω^2	j^2	$T/\lvert W\rvert$
1	0.98523	0.17126	0.087262	0.021741	0.35890
2	0.99375	0.11160	0.066105	0.029152	0.40345
3	0.99657	0.082750	0.052711	0.034638	0.42664
4	0.99784	0.065744	0.043714	0.039037	0.44084
5	0.99851	0.054534	0.037301	0.042740	0.45044
6	0.99891	0.046589	0.032513	0.045957	0.45736
7	0.99917	0.040664	0.028806	0.048814	0.46259
8	0.99935	0.036075	0.025854	0.051395	0.46667
9	0.99947	0.032417	0.023449	0.053755	0.46995
10	0.99957	0.029432	0.021451	0.055935	0.47265

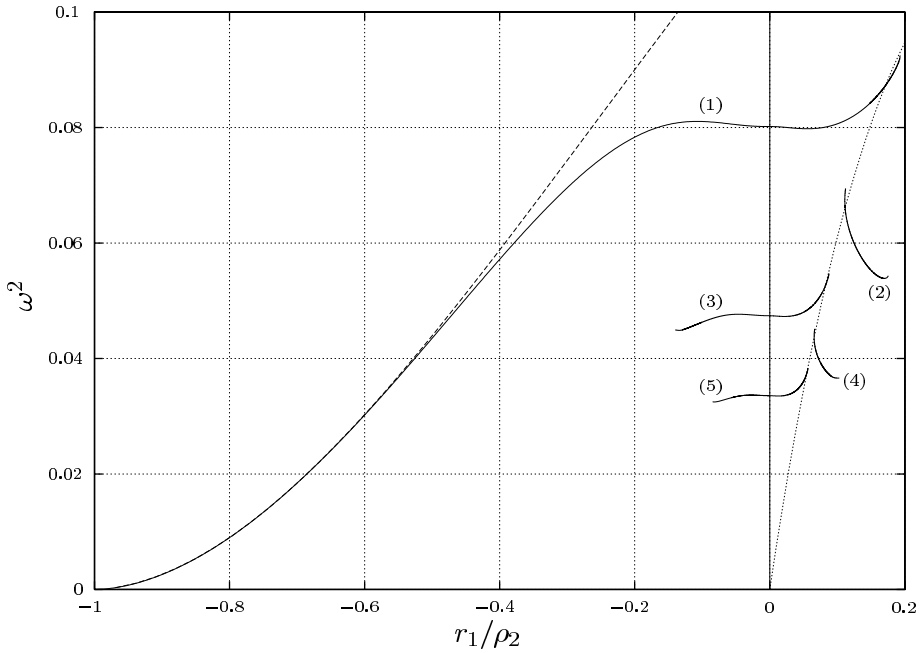

Figure 1. For the first five axisymmetric sequences (1), ... , (5), the squared angular velocity $\omega^2 = \Omega^2/(4\pi G\mu)$ is plotted against the radius ratio r_1/ρ_2, where $r_1 = \zeta_1$ (ζ_1 is the polar radius) for spheroidal figures and $r_1 = -\rho_1$ (ρ_1 is the inner equatorial radius) for toroidal shapes; ρ_2 is always the radius of the outer equatorial rim. The dotted curve represents the Maclaurin sequence and the dashed one corresponds to the Dyson approximation.

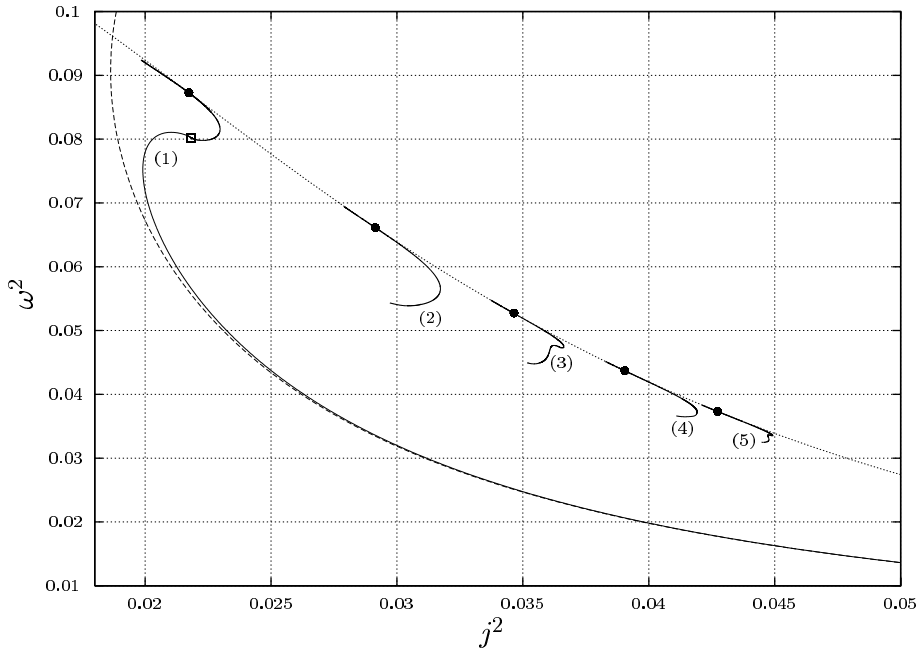

Figure 2. For the first five axisymmetric sequences, the squared angular velocity $\omega^2 = \Omega^2/(4\pi G\mu)$ is plotted against the dimensionless squared angular momentum j^2, given in formula (7). Dotted and dashed curves again refer to the Maclaurin sequence and the Dyson approximation respectively. The full circles mark the bifurcation points on the Maclaurin sequence, and the open square the transition configuration of spheroidal to toroidal bodies on the Dyson ring sequence.

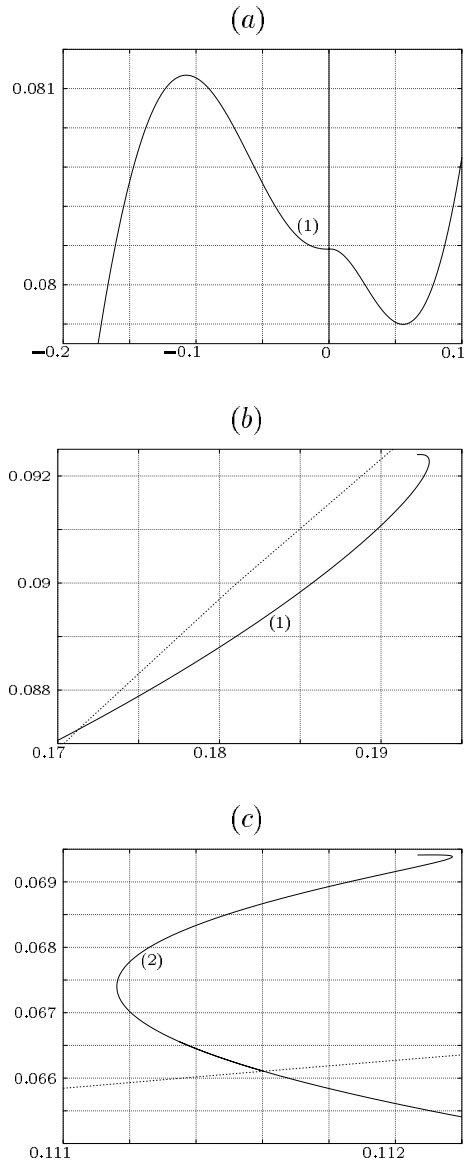

Figure 3. Magnified details of Fig. 1. The axes of the abscissae and ordinates have been stretched by a different factor.

over the fluid body V can be reduced to a one-dimensional integral as follows (Hill & Wheeler 1953; Wong 1974):

$$\Phi(\rho,\zeta) = -G\mu \int_{\rho_1}^{\rho_2} \int_{-\zeta_s(\rho')}^{\zeta_s(\rho')} \int_0^{2\pi} \frac{\rho'\,\mathrm{d}\phi'\,\mathrm{d}\zeta'\,\mathrm{d}\rho'}{\sqrt{\rho^2+\rho'^2+(\zeta-\zeta')^2-2\rho\rho'\cos\phi'}}$$

$$= -4G\mu \int_{\rho_1}^{\rho_2} \int_{-\zeta_s(\rho')}^{\zeta_s(\rho')} \frac{\rho' K(m)\,\mathrm{d}\zeta'\,\mathrm{d}\rho'}{\sqrt{(\rho+\rho')^2+(\zeta-\zeta')^2}} \tag{5}$$

$$= -2G\mu \int_{\rho_1}^{\rho_2} [A_-(\rho';\rho,\zeta) - A_+(\rho';\rho,\zeta)]\rho'\,\mathrm{d}\rho' \tag{6}$$

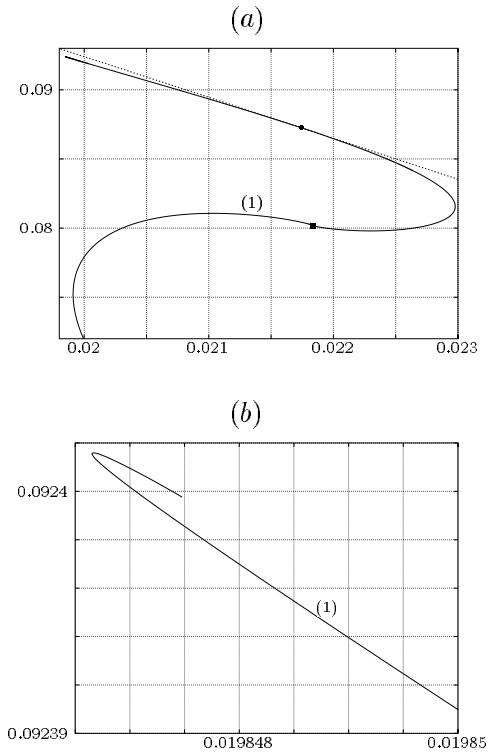

Figure 4. Magnified details of Fig. 2. The axes of the abscissae and ordinates have been stretched by a different factor.

with

$$A_\pm(\rho';\rho,\zeta) = \frac{\pm[(\rho+\rho')K(m_\pm) - 2\rho D(m_\pm)]\zeta_s'(\rho') + [\zeta \mp \zeta_s(\rho')]K(m_\pm)}{\sqrt{(\rho+\rho')^2+[\zeta\mp\zeta_s(\rho')]^2}}.$$

In these expressions the surface is described by a non-negative function ζ_s defined on the interval $[\rho_1, \rho_2]$ and $\zeta_s{}'$ denotes its first derivative. Note that $\rho_1 = 0$ for a spheroidal equilibrium figure, whereas for a toroidal figure ρ_1 denotes the inner equatorial radius; ρ_2 is always the radius of the outer equatorial rim.

The functions K and D are defined by the elliptic integrals

$$K(m) = \int_0^{\pi/2} \frac{\mathrm{d}\alpha}{\sqrt{1-m^2\sin^2\alpha}},$$

$$D(m) = \int_0^{\pi/2} \frac{\sin^2\alpha\,\mathrm{d}\alpha}{\sqrt{1-m^2\sin^2\alpha}},$$

and the modulus is given by

$$m = \sqrt{\frac{4\rho\rho'}{(\rho+\rho')^2+(\zeta-\zeta')^2}}$$

$$m_\pm = \sqrt{\frac{4\rho\rho'}{[\rho+\rho']^2+[\zeta\mp\zeta_s(\rho')]^2}}$$

in expressions (5) and (6) respectively.[2]

Inserting the integral expression (6) into the surface condition (2), one gets a non-linear integral equation for the unknown shape of the

[2] Writing (6) as a contour integral over a vector field and using Stokes' integral theorem as well as functional relations between elliptic integrals, one arrives at the expression (5).

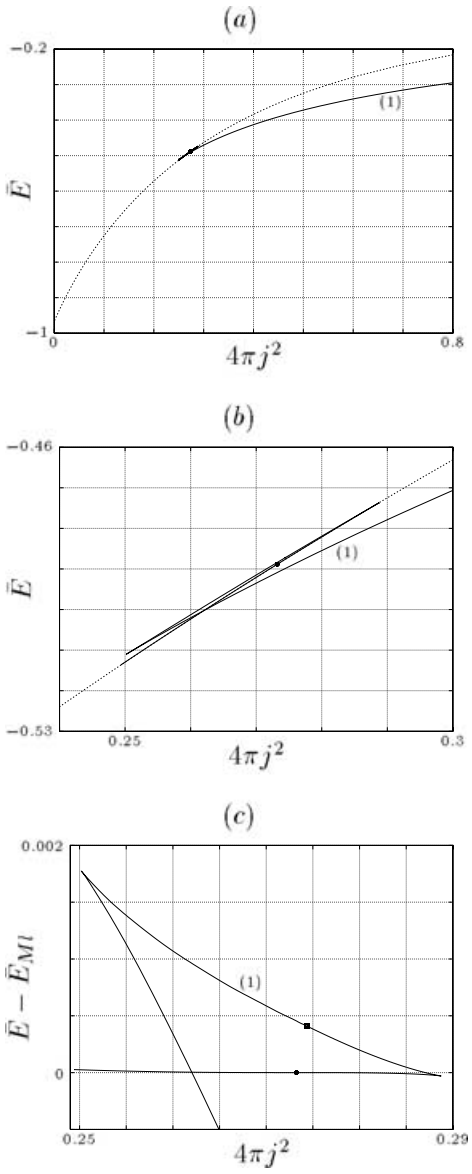

Figure 5. For the Dyson ring sequence, the dimensionless total energy $\bar{E}$, given in formula (8), is plotted against $4\pi j^2$ (see equation 7). The Maclaurin sequence is indicated by the dotted curve; the full circle marks the corresponding bifurcation point. The diagram (b) shows a magnified detail of (a), again with different stretching factors for the two axes. In (c), the difference $(\bar{E} - \bar{E}_{MI})$ of the respective energies of Dyson ring configurations and Maclaurin solutions belonging to the same j^2 is displayed. The empty square marks the transition configuration of spheroidal to toroidal bodies.

body's surface, which is uniquely soluble at least in the vicinity of some given solution if an appropriate triple of parameters is prescribed.[3] We write the shape of the body's surface parametrically in terms of a Chebyshev expansion in the following manner:

[3] As an example, the density μ, the angular velocity Ω and the constant Φ_0 of the fluid body can be taken. However, at the bifurcation points ε_k it is necessary to use different parameters, in order to assure a unique solution – see below.

Table 2. Physical quantities for the ε_1 configurations (A), ..., (L) displayed in Fig. 6. The abbreviations 'MSL' and 'MLS' refer to the mass-shedding limit and the Maclaurin spheroid respectively.

r_1/ρ_2	ω^2	j^2	$T/\lvert W\rvert$	
0.19224	0.092400	0.019847	0.34379	(A): MSL
0.18500	0.089834	0.020815	0.35175	(B)
0.17126	0.087262	0.021741	0.35890	(C): MLS
0.16000	0.085614	0.022260	0.36249	(D)
0.13000	0.082464	0.022927	0.36549	(E)
0.10000	0.080648	0.022898	0.36260	(F)
0.050000	0.079809	0.022215	0.35404	(G)
0.000000	0.080181	0.021836	0.35047	(H)
−0.20000	0.078338	0.020036	0.32825	(I)
−0.40000	0.057176	0.021726	0.31082	(J)
−0.60000	0.030207	0.031052	0.31542	(K)
−0.80000	0.0089862	0.063778	0.33800	(L)

$$\rho_s(\tau) = \sqrt{\rho_1^2 + \left(\rho_2^2 - \rho_1^2\right)\tau},$$

$$\zeta_s[\rho_s(\tau)] = \sqrt{(1-\tau)\left[\zeta_1^2 + \tau g(\tau)\right]},$$

$$g(\tau) = \sum_{k=1}^{\infty} g_k T_{k-1}(2\tau - 1) - \tfrac{1}{2} g_1,$$

$$T_k(x) = \cos(k \arccos x).$$

The variable τ runs over the interval [0, 1], and the parameter ζ_1 represents the polar radius for spheroidal figures and $\zeta_1 = 0$ for toroidal shapes.

If we prescribe μ, Ω and Φ_0, restrict ourselves to a finite number $(N - 2)$ of coefficients g_k and take the surface condition (2) at the N surface points $(\rho_s(\tau_k), \zeta_s[\rho_s(\tau_k)])$ with $T_N(2\tau_k - 1) = 0$, the integral equation in question turns into a system of N equations for the unknown coefficients g_k and the likewise unknown quantities r_1 and ρ_2, where r_1 stands for ζ_1 in the spheroidal and for $(-\rho_1)$ in the toroidal case. Alternatively, we can prescribe the value $g(\tau = 1)$ and search instead for Φ_0. A choice $g(1) \neq 0$ assures a unique solution at the desired ε_k sequence if we are in the vicinity of ε_k. This is due to the fact that for all Maclaurin solutions $g(\tau)$ is identically zero.

The solution of the remaining system of N equations can be found by means of a Newton–Raphson method. The Maclaurin spheroids at the bifurcation points serve as initial solutions, and by choosing $g(1) < 0$ we move towards the mass-shedding limit of the respective sequence, whereas $g(1) > 0$ yields the path towards the ring or core–ring structures (see Section 4). The mass-shedding limit is reached when $g(1) = -\zeta_1^2$, which leads to a cusp at the equatorial rim of the body. Although for this configuration derivatives of the above function g are singular at $\tau = 1$ (which results in a loss of accuracy, see below), we can choose $g(1)/\zeta_1^2$ as one of our parameters and can thus place ourselves precisely on this point.

Once upon the sequence and sufficiently far away from the Maclaurin sequence, we may change the parameter prescription, e.g. to the triples (μ, Ω, Φ_0) or $(\mu, r_1/\rho_2, \Phi_0)$. Note that rapid convergence of this method towards the actual shape of the body, as N grows, requires, for a given set of coefficients g_k, a highly accurate evaluation of the integral expression (6). This is done by dividing the interval [0, 1] into many sub-intervals, which are extremely small in the vicinity of the respective zero τ_k and grow exponentially as one moves away from τ_k. Moreover, for $m \approx 1$ the elliptic integrals are written in logarithmic expansions (see Gradstein & Ryshik 1981, p. 295ff.). Additionally, special care is taken for surface points close

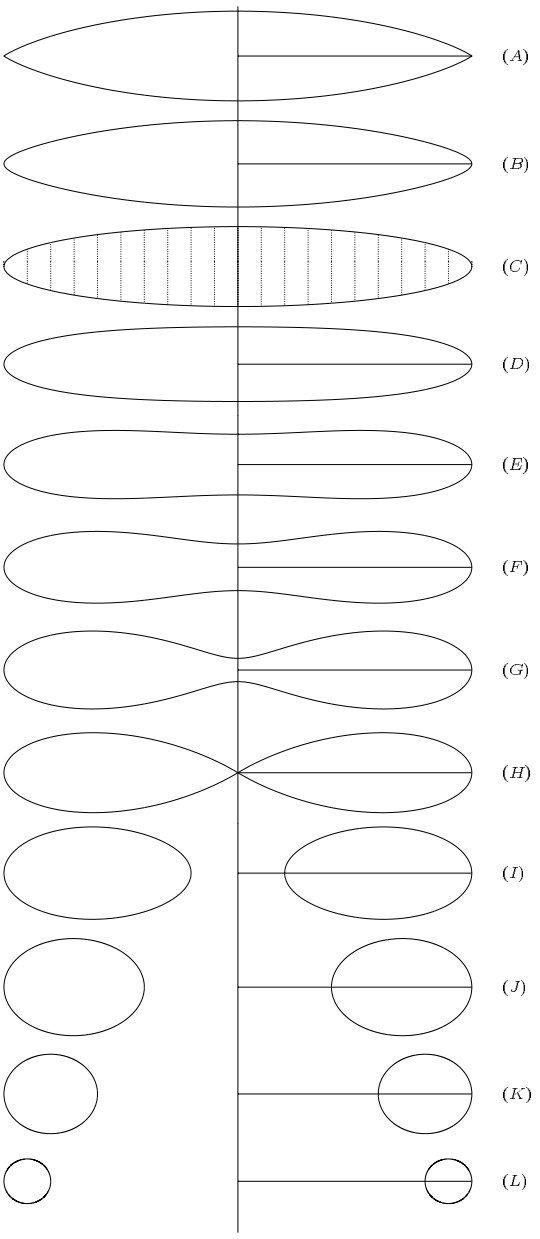

Figure 6. Meridional cross-sections of configurations belonging to the ε_1 sequence – see Table 2. The dimensionless quantity ζ/ρ_2 is plotted against ρ/ρ_2. The Maclaurin body is denoted by hatching.

to the equatorial plane. In this manner we achieve an accuracy of up to 12 digits for intermediate solutions that are sufficiently far away from the mass-shedding limit as well as from any transition body where the topology of the figure changes. The loss of accuracy as one approaches these critical configurations comes about since derivatives of g become singular at a certain point[4] on the body's surface. However, we are still able to obtain an accuracy of five digits for all physical quantities given in Tables 2–5.

[4] This critical point is the equatorial rim for the mass-shedding configuration, the 'pinching' point for the configuration at which the two-body system forms and the origin $\rho = 0 = \zeta$ for the transition body of spheroidal to toroidal figures.

Table 3. Physical quantities for the ε_2 configurations (A), ..., (L) displayed in Fig. 7. The abbreviations 'MSL', 'MLS' and '2BS' refer to the mass-shedding limit, the Maclaurin spheroid and the formation of the two-body system respectively.

r_1/ρ_2	ω^2	j^2	$T/\|W\|$	
0.11207	0.069411	0.027909	0.39710	(A): MSL
0.11140	0.068335	0.028310	0.39919	(B)
0.11160	0.066105	0.029152	0.40345	(C): MLS
0.11300	0.064738	0.029663	0.40587	(D)
0.11500	0.063529	0.030101	0.40779	(E)
0.12000	0.061475	0.030787	0.41032	(F)
0.12500	0.059960	0.031218	0.41132	(G)
0.13000	0.058718	0.031496	0.41137	(H)
0.13500	0.057661	0.031659	0.41067	(I)
0.14500	0.055961	0.031701	0.40744	(J)
0.15500	0.054729	0.031417	0.40219	(K)
0.17558	0.054327	0.029720	0.38610	(L): 2BS

Table 4. Physical quantities for the ε_3 configurations (A), ..., (L) displayed in Fig. 8. The abbreviations 'MSL', 'MLS' and '2BS' refer to the mass-shedding limit, the Maclaurin spheroid and the formation of the two-body system respectively.

r_1/ρ_2	ω^2	j^2	$T/\|W\|$	
0.087646	0.054735	0.033738	0.42327	(A): MSL
0.086000	0.053836	0.034134	0.42477	(B)
0.082750	0.052711	0.034638	0.42664	(C): MLS
0.075000	0.050871	0.035462	0.42947	(D)
0.060000	0.048799	0.036307	0.43162	(E)
0.040000	0.047554	0.036625	0.43116	(F)
0.020000	0.047289	0.036544	0.42979	(G)
0.000000	0.047391	0.036458	0.42932	(H)
−0.050000	0.047666	0.036216	0.42800	(I)
−0.10000	0.046297	0.036022	0.42281	(J)
−0.12000	0.045352	0.035860	0.41895	(K)
−0.13998	0.044952	0.035174	0.41220	(L): 2BS

4 RESULTS

The evolutions of the five sequences bifurcating at the eccentricities $\varepsilon_1, \ldots, \varepsilon_5$ are displayed in Figs 1 and 2, where $\omega^2 = \Omega^2/(4\pi G\mu)$ is plotted against the ratio r_1/ρ_2 and against the dimensionless angular momentum j^2 defined by

$$j^2 = \frac{J^2\mu^{1/3}}{4\pi G M^{10/3}}, \tag{7}$$

where M and J are the mass and the angular momentum of the body, respectively. The corresponding (dotted) curves of the Maclaurin spheroids are given as well as the analytic Dyson approximation of the ε_1 sequence (dashed lines).

In Fig. 1, the bifurcation points appear as cross-over points of the Maclaurin and respective ε_k sequence. One end of a particular sequence is marked by a mass-shedding limit, always possessing a higher angular velocity ω^2 compared to the other end. The details of the typical evolution of a particular sequence can be seen in Fig. 3. A characteristic feature of all sequences is the occurrence of a local maximum in ω^2 close to the mass-shedding limit – see Figs 3(b), (c) and 4(b).

All ε_{2l-1} sequences show the transition of a spheroidal to a toroidal figure, and ω^2 possesses a local minimum and maximum before and after this point respectively – see also Figs 3(a) and 4(a). Another

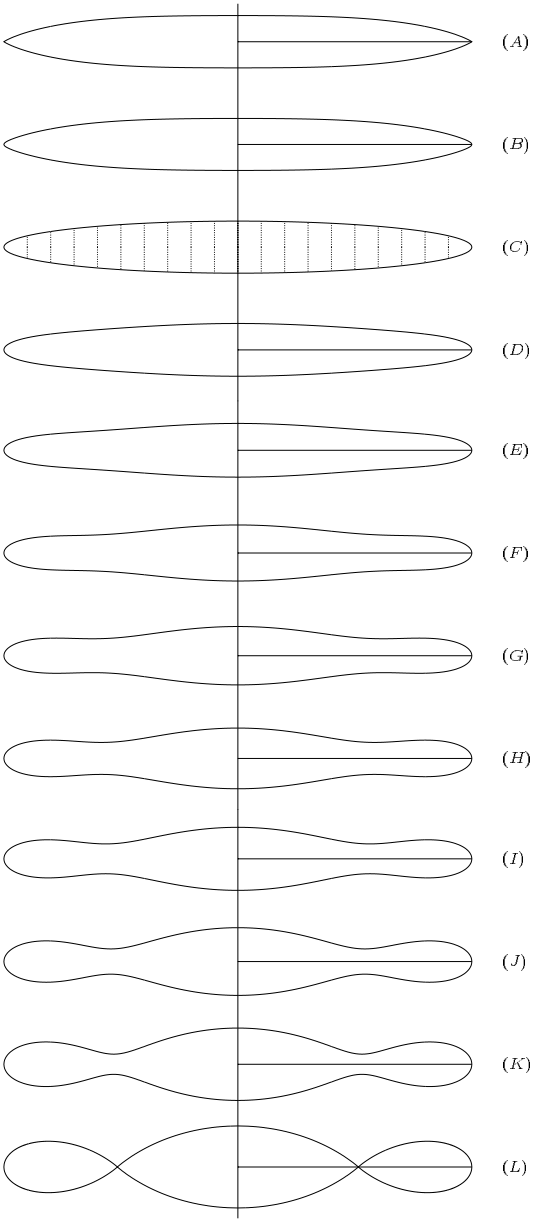

Figure 7. Meridional cross-sections of configurations belonging to the ε_2 sequence – see Table 3. The dimensionless quantity ζ/ρ_2 is plotted against ρ/ρ_2. The Maclaurin body is denoted by hatching.

typical property is the vanishing gradient of ω^2 as a function of r_1/ρ_2 as well as a discontinuous change of the sign of its curvature at $r_1/\rho_2 = 0$. Apart from the ε_1 sequence, the paths end with the formation of a two-body system, namely a core and a ring for $k = 2l$ and two rings if $k = 2l + 1$. Shortly before coming to this end, a minimum in ω^2 occurs, which becomes less and less pronounced as one moves to higher values of k.

As depicted by Hachisu & Eriguchi (1983), the paths of the ε_k sequences glance off the Maclaurin sequence,[5] if one plots ω^2 against j^2 (see Fig. 2). Representative details corresponding to the ε_1 curve can be seen in Fig. 4. Note the extraordinary accuracy needed in order to resolve the global maximum in ω^2 close to the mass-shedding limit displayed in Fig. 4(b).

[5] At the bifurcation points the slopes are identical.

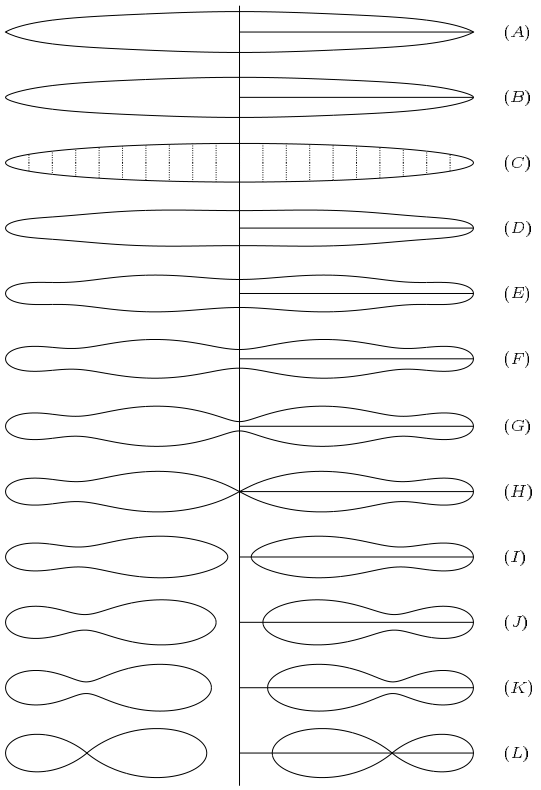

Figure 8. Meridional cross-sections of configurations belonging to the ε_3 sequence – see Table 4. The dimensionless quantity ζ/ρ_2 is plotted against ρ/ρ_2. The Maclaurin body is denoted by hatching.

Table 5. The ratios M_1/M_2 of the masses of the inner to the outer body at the two-body formation point for the $\varepsilon_2, \ldots, \varepsilon_5$ sequences.

	(2)	(3)	(4)	(5)
M_1/M_2	0.41051	0.86563	1.7235	2.4987

In Figs 1 and 2, moreover, the analytic curves of the Dyson approximation can be found. With the assumption of circular cross-sections of the toroids as $\rho_1/\rho_2 \to 1$, one may expand (5) in terms of $(1 - \rho_1/\rho_2)$ and find by means of (2) an expansion of the toroids' surfaces. Dyson went to a fourth-order approximation, resulting in excellent agreement with the numerical results[6] for large ρ_1/ρ_2.

Fig. 5(a) is a replot of fig. 1 from Bardeen (1971), with the Dyson approximation being replaced by the actual evolution of the ε_1 sequence. Here, the dimensionless total energy $\bar{E}$ is given by

$$\bar{E} = \frac{T + W}{G\mu^{1/3}M^{5/3}} = 2\pi j\omega \left(1 + \frac{W}{T}\right), \tag{8}$$

with the kinetic and gravitational energies

$$T = \tfrac{1}{2}J\Omega \qquad \text{and} \qquad W = \tfrac{1}{2}\mu \int_V \Phi \, \mathrm{d}^3\boldsymbol{r} = \tfrac{3}{5}M\Phi_0 + T.$$

The latter formula follows from the virial theorem

$$2T + W + 3\int_V p \, \mathrm{d}^3\boldsymbol{r} = 0,$$

[6] In our computations, we compared configurations with the same ρ_1, ρ_2 and μ.

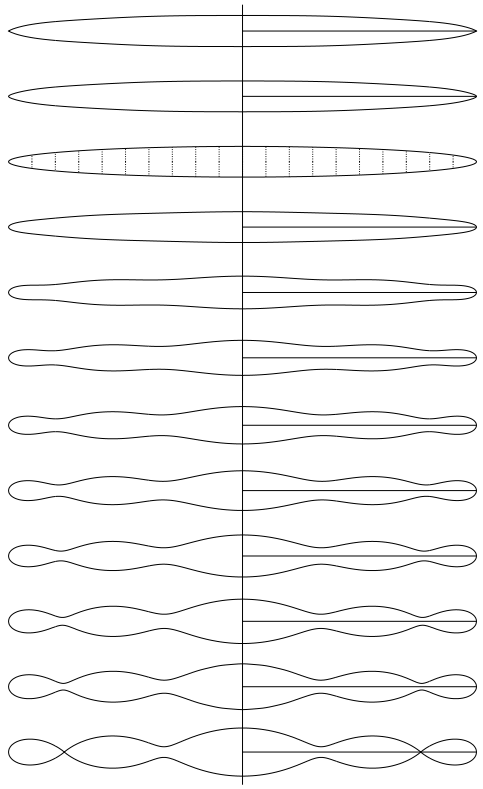

Figure 9. Meridional cross-sections of configurations belonging to the ε_4 sequence. The dimensionless quantity ζ/ρ_2 is plotted against ρ/ρ_2. The Maclaurin body is denoted by hatching.

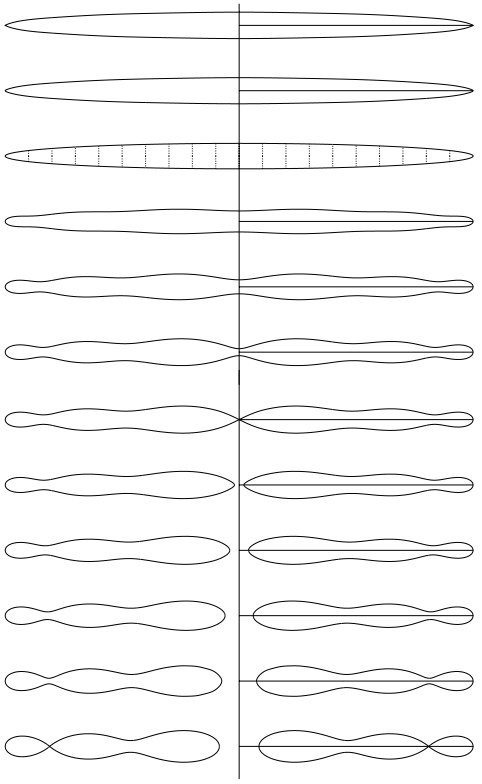

Figure 10. Meridional cross-sections of configurations belonging to the ε_5 sequence. The dimensionless quantity ζ/ρ_2 is plotted against ρ/ρ_2. The Maclaurin body is denoted by hatching.

which is valid for all stationary rotating fluid bodies, and from the hydrodynamical Euler equation, giving for a uniformly rotating homogeneous configuration the pressure p as

$$p = \mu\left(\Phi_0 - \Phi + \tfrac{1}{2}\Omega^2\rho^2\right).$$

Fig. 5(a) led Bardeen to the conjecture that the Dyson ring sequence branches off from the Maclaurin sequence exactly at the ε_1 bifurcation point, marked in Fig. 5 by the full circle symbol. However, a magnified detail of the plot in question shows a completely different picture, as can be seen in Figs 5(b) and (c). Coming from the toroidal end, the ε_1 sequence intersects the Maclaurin sequence close to but not exactly at the bifurcation point. As can be seen in Fig. 5(c), the ε_1 sequence intersects the Maclaurin sequence one more time before it moves on to the bifurcation point and beyond to the mass-shedding limit.[7] It is rather surprising that from this entangled picture the correct connections of the Dyson ring and the Maclaurin sequence could be drawn.

Table 2 contains numerical data, accurate to five digits, for physical quantities belonging to the ε_1 sequence. The corresponding meridional cross-sections of these bodies are displayed in Fig. 6. The intermediate Maclaurin body (C) is denoted by hatching. Note

[7] The relation $\mathrm{d}\bar{E} = 4\pi\omega\mathrm{d}j$, which is valid along any equilibrium sequence of uniformly rotating homogeneous fluid bodies (cf. Hartle & Sharp 1967; Bardeen 1971), explains two features of Fig. 5: the occurrence of cusps and the fact that the slope of the ε_1 sequence is identical to that of the Maclaurin sequence at the bifurcation point. Moreover, together with the coinciding slopes in the ω^2–j^2 plane (Fig. 2), one can conclude that the second derivatives in the $\bar{E}$–j^2 plane (Fig. 5) are identical at the bifurcation point as well.

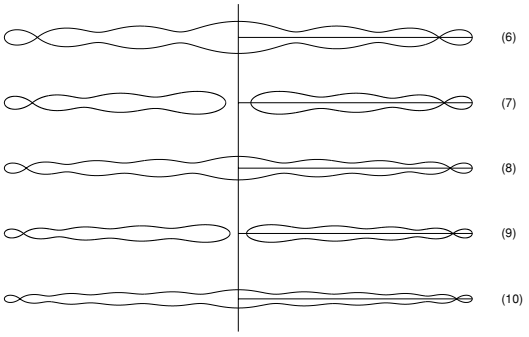

Figure 11. The formation of the two-body system at the end of the ε_6, $\ldots$, ε_{10} sequences.

that a lens-shaped configuration (B) appears that looks similar to the relativistic homogeneous fluid body displayed in fig. 1(a) of Ansorg, Kleinwächter & Meinel (2002). Additionally, the values of physical quantities like j^2 and ω^2 are similar for the two bodies.[8] Such a neighbourhood can also be found for the configurations (F) and fig. 1(b) of Ansorg et al. (2002).

Likewise, Tables 3 and 4 list data for the fluid bodies shown in Figs 7 and 8. Again, there is a configuration (B) of the ε_2 sequence (see Fig. 7) that is in the vicinity of a relativistic body, (c) in fig. 1 of Ansorg et al. (2002). Note the hint of a minimum at the north pole of the relativistic figure. Also for the configuration (B), this property is suggested by the linear surface displacement (4). However, as can be seen in Figs 6–10, the Newtonian configurations in between the Maclaurin body and the mass-shedding limit generate neither a

[8] In Ansorg et al. (2002), $j^2 = R/(4\pi)$ and $\omega^2 = \bar{\Omega}^2/(4\pi)$.

central bulge (which one would expect for the ε_{2l-1} sequences) nor a central minimum region (which would follow for the ε_{2l} sequences). However, in the general relativistic vicinity of these solutions, at least the latter property seems to show up.

Table 5 lists the ratios of the masses of the inner to the outer body at the two-body formation point for the $\varepsilon_2, \ldots, \varepsilon_5$ sequences.

Figs 9 and 10 display configurations of the ε_4 and ε_5 sequences, and Fig. 11 is devoted to the formation of the final two-body system for the $\varepsilon_6, \ldots, \varepsilon_{10}$ sequences. As mentioned in the Introduction, for ε_{2l} the resulting configuration consists of a corrugated central core region and an outer ring that just pinches off. Likewise, for ε_{2l+1} a two-ring system is formed.

An interesting open question concerns the behaviour of the ε_k sequences as k tends to infinity, corresponding to the disc limit ($\varepsilon \to 1$) of the Maclaurin spheroids.

ACKNOWLEDGMENTS

The authors would like to thank David Petroff for many valuable discussions. This work was supported by the Deutsche Forschungsgemeinschaft (DFG-project ME 1820/1).

REFERENCES

Ansorg M., Kleinwächter A., Meinel R., 2002, A&A, 381, L49
Bardeen J. M., 1971, ApJ, 167, 425
Chandrasekhar S., 1967, ApJ, 147, 334
Chandrasekhar S., 1969, Ellipsoidal Figures of Equilibrium. Yale Univ. Press, New Haven, CT
Dyson F. W., 1892, Phil. Trans. R. Soc., 184, 43
Dyson F. W., 1893, Phil. Trans. R. Soc., 184A, 1041
Eriguchi Y., Hachisu I., 1982a, Prog. Theor. Phys., 67, 844
Eriguchi Y., Hachisu I., 1982b, Prog. Theor. Phys., 67, 1068
Eriguchi Y., Hachisu I., 1985, A&A, 148, 289
Eriguchi Y., Sugimoto D., 1981, Prog. Theor. Phys., 65, 1870
Gradstein I. S., Ryshik I. M., 1981, Tables of Series, Products, and Integrals. Harry Deutsch Thun, Frankfurt/Main
Hachisu I., Eriguchi Y., 1983, MNRAS, 204, 583
Hartle J. B., Sharp D. H., 1967, ApJ, 147, 317
Hill D. L., Wheeler J. A., 1953, Phys. Rev., 89, 1102
Kley W., 1996, MNRAS, 282, 234
Kowalewsky S., 1895, Astron. Nachr., 111, 37
Lichtenstein L., 1933, Gleichgewichtsfiguren rotierender Flüssigkeiten. Springer, Berlin
Morse P. M., Feshbach H., 1953, Methods of Theoretical Physics. McGraw-Hill, New York
Poincaré H., 1885a, C. R. Acad. Sci., 100, 346
Poincaré H., 1885b, Bull. Astron., 2, 109
Poincaré H., 1885, Bull. Astron., 2, 405
Wong C. Y., 1974, ApJ, 190, 675

This paper has been typeset from a TEX/LATEX file prepared by the author.